ACS OMEGA

Open Access

http://pubs.acs.org/journal/acsodf

Article

Insights into Tetravalent Np Speciation in HNO_3 through Spectroelectrochemistry and Multivariate Analysis

Sara E. Gilson, Hunter B. Andrews, Luke R. Sadergaski,* and Adam J. Parkison

Cite This: *ACS Omega* 2024, 9, 43547−43556

Read Online

ACCESS | Metrics & More | Article Recommendations | Supporting Information

ABSTRACT: In situ optical spectroscopy, spectropotentiometry, and multivariate analysis were applied to the Np(IV) nitrate system to better understand speciation and quantify HNO_3 concentration. Thin-layer spectropotentiometry, or spectroelectrochemistry, was leveraged to isolate and stabilize Np(IV) without compromising the solution conditions and generate representative Vis-NIR absorption spectra from 0.5 to 10 M HNO_3 and benchmark the corresponding Np(IV) molar absorptivity coefficients. Spectra were described with principal component analysis (PCA) to identify the purest Np(IV) absorbance spectra among other oxidation states [e.g., Np(V/VI)] at each acid concentration and then to identify the primary sources of variance within each Np(IV) spectrum with respect to Np(IV) nitrate complexes. Then, partial least-squares regression (PLSR) and support vector regression (SVR) models were built to predict HNO_3 concentration from the Np(IV) spectral data. The nonlinear SVR model outperformed the linear PLSR model for the HNO_3 concentration predictions. Finally, the inclusion of spectra collected in edge and center point HNO_3 concentrations in the calibration set was determined to be crucial for producing models with strong predictive capabilities. The multivariate approach used in this study makes it possible to quantify HNO_3 concentration solely based on Np(IV) absorption spectra, which is essential to quantifying processing streams in various online monitoring applications.

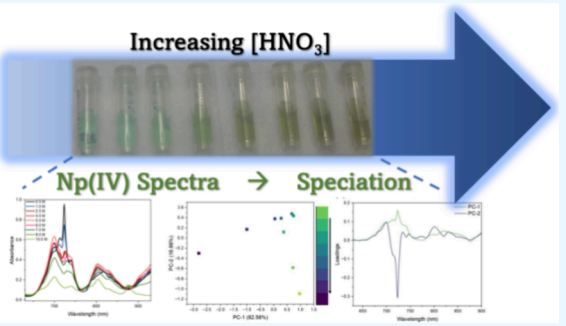

INTRODUCTION

Radiochemical separations, such as those used for the purification of the heat source ^{238}Pu, typically involve separating actinides in acidic solutions under harsh radioactive environments. Numerous factors influence the efficiency and outcome of these separations, such as metal ion concentration, actinide oxidation state, acid concentration, and temperature. Online monitoring of these processes via optical spectroscopy can provide rapid, in situ information to inform key processing decisions.[1−3] Techniques such as absorption spectroscopy provide information about many of the factors that influence processing. Absorption spectroscopy, or spectrophotometry, is a powerful technique that can detect the presence of certain elements, elucidate electronic structure, describe coordination environment, and provide information about concentrations of species. This technique is especially relevant to the nuclear field because many of the actinide elements that are encountered in radioisotope processing provide unique absorbance spectra that can be used for identification and quantification in feed and product solutions.[4]

Spectrophotometry is particularly useful for studying early actinides such as Np. The element Np is capable of adopting multiple oxidation states that frequently coexist in solution and are highly dependent on solution conditions.[5] The most-studied oxidation states of Np are Np(IV), (V), and (VI), and each has characteristic electronic transitions that allow for qualitative identification and quantitative determination through univariate methods such as Beer's law in simple systems. However, when the spectrum of an oxidation state is highly sensitive to the coordination environment of the Np cation, spectral features can overlap, shift, or change significantly, making it challenging to identify the different species in a system.[6,7]

This is the case for Np(IV) in HNO_3, which is an exceptionally complex system because of changes in spectral features corresponding to the formation of various Np nitrato complexes with increasing HNO_3 concentration.[8−10] Nitrate groups coordinate the Np ion and displace coordinated water ligands as acid concentration increases; however, the speciation of Np(IV)—particularly at low to intermediate HNO_3 concentrations—remains uncertain despite numerous reports in the literature.[11]

In this study, we established a thin-layer spectroelectrochemistry approach to stabilize Np(IV) species near ∼0.1 M

Received: June 11, 2024
Revised: September 9, 2024
Accepted: September 16, 2024
Published: October 16, 2024

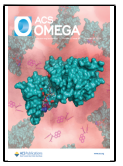

https://doi.org/10.1021/acsomega.4c05464
ACS Omega 2024, 9, 43547−43556

Np and collected absorption spectra over a wide range from 0.5 to 10 M HNO_3 to address experimental data vacancies and inconsistencies in the literature.[9−11] Emphasis was placed on collecting spectra in low HNO_3 acid concentrations (>4 M) and establishing molar absorptivity coefficients. The Np(IV) was stabilized by applying a controlled potential to each sample to preserve the targeted solution conditions. Corresponding molar absorptivity coefficients were calculated for the most significant absorbance bands in each spectrum. To explore Np(IV) nitrate speciation at given concentrations, principal component analysis (PCA) was applied as a data reduction technique. PCA is typically applied to data sets to help describe variance within the data by reducing it into orthogonal principal components (PCs).[7] Supervised regression models including linear partial least-squares regression (PLSR) and nonlinear support vector regression (SVR) models were also optimized for the quantification of HNO_3. More information on these chemometric techniques has been provided elsewhere.[4,12,13] The Np(IV) absorption spectra collected in this study were used in combination with previous literature to guide chemometric analyses and produce models that provide insight into Np(IV) speciation over this HNO_3 concentration range as well as quantify HNO_3 in unknown samples.

EXPERIMENTAL SECTION

Caution. The isotope ^{237}Np ($t_{1/2}$ = 2.14 × 10^6 years) is an α-emitting radionuclide. All work was conducted in facilities equipped to handle this radioisotope. Sample preparation and measurements were performed in a negative-pressure glovebox.

Chemicals. The Np nitrate solid was obtained in-house from the Oak Ridge National Laboratory. Milli-Q purity water (18.2 MΩ cm^{-1} at 25 °C) and concentrated HNO_3 (Merck, 65% for analysis) were used to prepare all solutions and samples.

Sample Preparation. The Np stock was prepared by dissolving a Np nitrate solid from Oak Ridge National Laboratory in 0.01 M HNO_3. To strip the ^{233}Pa daughter and ^{239}Pu impurities, a Dowex-50 cation exchange column (Sigma-Aldrich, Dowex-50×8, hydrogen form, 100−200 mesh) was used. To reduce Np to the pentavalent oxidation state, H_2O_2 was added to the Np solution. Then, the solution was loaded onto the column and the Np was eluted with 0.5 M HNO_3. The concentrations of the resulting Np stock solutions were determined via α-spectroscopy (Canberra Alpha Spectrometer Model 7401) and inductively coupled plasma mass spectrometry (ICP-MS) (iCAP Q ICP-MS, Thermo Fischer Scientific). These stock solutions were used to prepare all calibration and validation samples (0.08−0.17 M Np) through dilution with appropriate volumes of concentrated HNO_3 and Milli-Q water.

The compositions of the samples examined in this study are summarized in Table 1. Select sample compositions (denoted with an asterisk in Table 1) underwent acid−base titration to confirm [H^+] and alpha spectroscopy to determine total Np concentration. The ultraviolet (UV) region of the absorption spectra was monitored for characteristic HNO_2 peaks during spectral data collection.[14] Each sample was subsequently stored in a 2.0 mL plastic microcentrifuge tube. The measurements were performed within a reasonable time frame after sample prep to ensure that nitrite production was not an issue. Nitrite was not observed in any of the samples until after reducing potentials were applied.[14]

Table 1. Np Sample Target Compositions

sample	Np (g L^{-1})	HNO_3 (M)
Np S1	0.08	0.5
Np S2[a]	0.08	1.0
Np S3	0.08	2.5
Np S4[a]	0.08	4.0
Np S5	0.08	5.0
Np S6[a]	0.08	6.0
Np S7	0.08	7.0
Np S8[a]	0.08	8.0
Np S9	0.08	10.0
Np S10	0.02	3.5
Np S11	0.04	2.0
Np S12	0.17	5.5
Np S13	0.17	1.0

[a]Underwent acid−base titration to confirm [H^+].

Spectrophotometry. UV−visible (UV−vis) spectra were collected with a QEPro spectrophotometer (Ocean Insight), and near-infrared (NIR) spectra were collected by using a NIRQuest (Ocean Insight) spectrophotometer. A stabilized W−halogen lamp (ThorLabs) was used as the light source. UV−vis spectra were collected from 320 to 1115 nm every 0.80 nm, and NIR spectra were collected from 892 to 1700 nm every 1.59 nm. Spectra were averaged accordingly to optimize the signal-to-noise ratio and were collected continuously throughout the experiment. Spectrochemical measurements were conducted using a 1.75 mm path length cuvette with a screen-printed Pt honeycomb working electrode (Pine Research), Ag/AgCl micro reference electrode (Pine Research), and an SP-300 BioLogic potentiostat. Electrochemical scans gradually reduced Np in solution from Np(VI/V) to Np(IV). For most samples, this reduction took place at an applied potential of approximately 0.05 V vs Ag/AgCl.

Small volumes (320 μL) of sample were pipetted into the cuvette and spectra were checked for any anomalous signals. A general strategy was used to increase the potential to oxidize the Np to the hexavalent oxidation state. Once the cell current stabilized, the potential was systematically decreased with the goal of stabilizing Np(IV) and collecting absorption spectra. For the samples prepared at higher acidities (>4 M HNO_3), solvent interference was encountered, likely because of H_2 evolution, and a modified method was used to skip certain potential ranges and avoid this issue.[10,11] For HNO_3 concentrations of 4 M and higher, the potential range from approximately 0.5−0.1 V (vs Ag/Ag/Cl) was avoided to prevent side reactions from occurring and disrupting the spectroscopic signal.

Multivariate Data Analysis. Multivariate analyses were conducted on spectra that were baseline corrected by subtracting the minimum absorbance value (between 630 and 1030 nm for the UV−vis spectra and between 900 and 1030 nm for the NIR data) and the mean-centered.

PCA served multiple purposes in this study. First, it was used as a data reduction technique to identify sources of variance in the signal matrices (the spectra) for each of the calibration set samples (Np S1−S9). The use of PCA on Np absorbance spectra for data reduction has been reported previously.[15] This method allowed for the selection of the Np(IV) end point UV−vis and NIR spectra from large data sets for each sample (see Figure S2). Then, two data sets were assembled consisting of only the Np(IV) end point UV−vis

https://doi.org/10.1021/acsomega.4c05464
ACS Omega 2024, 9, 43547−43556

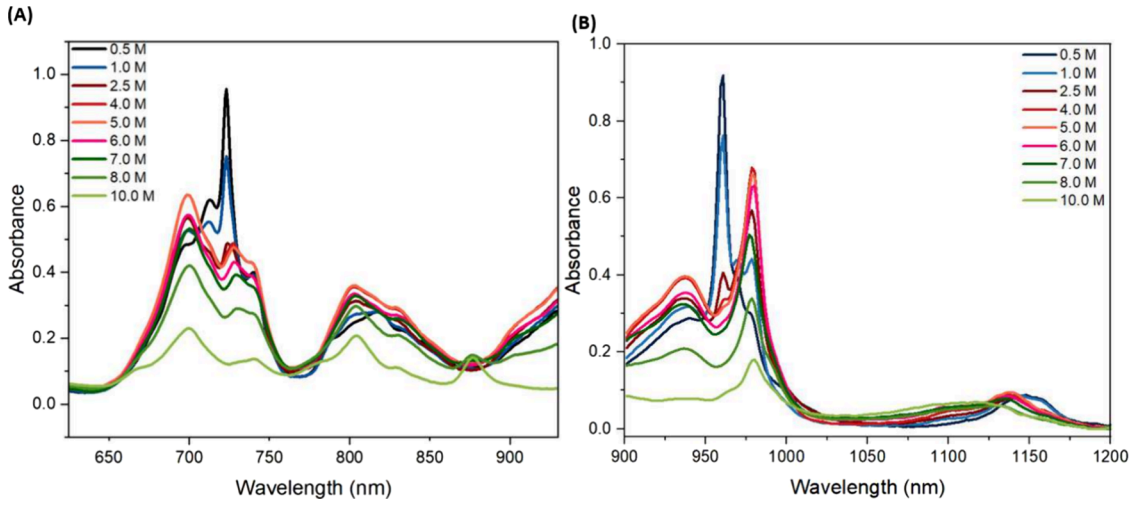

Figure 1. PCA-guided UV−vis (A) and NIR (B) spectra of 0.08 M Np in the Np(IV) state in 0.5−10 M HNO_3.

and NIR spectra for each of the calibration set samples. PCA models were built and used for data exploration of these spectra, with the goal of gaining insight into Np(IV) speciation. When PCA models were built, only a baseline correction was applied to the spectral data.

PLSR is a supervised factor analysis method that has been used with great success for many decades to find the structure in X (e.g., spectra) that is most predictive for Y (e.g., concentration matrix).[12,16] PLSR models were built with the optimal number of latent variables (LVs) corresponding to the model with the last significant decrease in the root-mean-square error (RMSE) of the cross-validation (CV). PLS-1 models were generated with one Y variable for HNO_3 concentrations. Both k-fold (k = 5) and leave-one-out CV strategies were evaluated.

SVR is a type of support vector machine that can be applied to regression problems. SVR minimizes RMSE using linear and nonlinear kernels.[13,17,18] SVR handles outliers well and is less prone to overfitting compared with PLSR. SVR models require careful parameter selection and often need larger data sets than PLSR. In this study, a linear SVR parameter did not perform well with this data set. A third-order polynomial was sufficient to build robust models and maintain the computation time. The software created a heat map of the RMSE versus the two hyperparameters (γ and ε). Blue regions indicate strong performance and red regions indicate poor RMSE metrics. Moderate ε and γ values near the center of the heat maps were selected to minimize overfitting and underfitting. PCA, PLSR, and SVR models were built and tested by using the software package Vektor Direktor (2.0) from the KAX Group. The Unscrambler X software version 10.4 (Camo Analytics AS, Oslo, Norway) was used for multivariate curve resolution.

Model performance was evaluated by using calibration, CV, and prediction metrics. The primary statistics used to evaluate the model performance were the RMSE of the calibration (RMSEC), the RMSE of the cross-validation (RMSECV), and RMSE of the prediction (RMSEP). RMSEs were calculated using eq 1:

$$\mathrm{RMSE} = \sqrt{\frac{\sum_{i=1}^{n} (\hat{y}_i - y_i)^2}{n}} \quad (1)$$

where $\hat{y}_i$ is the predicted concentration, y_i is the measured concentration, and n is the number of samples. All RMSE values were converted to percent values for easier comparisons by dividing the RMSEP by the average model values using eq 2:

$$\mathrm{RMSEP\%} = \frac{\mathrm{RMSEP}}{y_{\mathrm{med}}} \times 100\% \quad (2)$$

where y_{med} represents the average of each analyte concentration range. RMSE values are in units of analyte concentration, and lower RMSEP values indicate better model performance.

RESULTS AND DISCUSSION

Np Absorbance Spectra. Spectral data sets were generated from the spectroelectrochemical experiments of the samples listed in Table 1. The electrochemical stabilization of the majority of the tetravalent Np oxidation state was achievable for these samples. Representative spectra highlighting the characteristic spectral features of Np(IV) are given in Figure 1, with full spectra given in the Supporting Information (SI) (Figure S1). These spectra were selected from other larger spectral data sets generated during spectroelectrochemical scans using PCA. PCA was used for data reduction and guided the selection of the Np(IV) end point spectra in Figure 1 using the PCA scores plot (see Figure S2). Our data are generally consistent with those reported previously,[8−10] although it is worth noting that spectra from the literature have typically focused on rather narrow acid ranges and used different methods (chemical and electrochemical) to stabilize Np(IV) in solution. Differences in the absorbance spectra of Np(IV) stemming from chemical or electrochemical stabilization have not been well-studied.

Spectral features in Figure 1 change significantly with increasing HNO_3 concentration, as has been reported in the literature.[8−10] Nitrate is a coordinating ligand, and extended X-ray absorption fine structure (EXAFS) studies of Np in nitrate media have suggested that nitrate groups gradually replace coordinated water molecules as nitrate concentration increases.[5,11] This change in the coordination environment of the Np(IV) cation in solution is reflected in its absorbance spectra with increasing HNO_3 concentration. Certain elec-

https://doi.org/10.1021/acsomega.4c05464
ACS Omega 2024, 9, 43547−43556

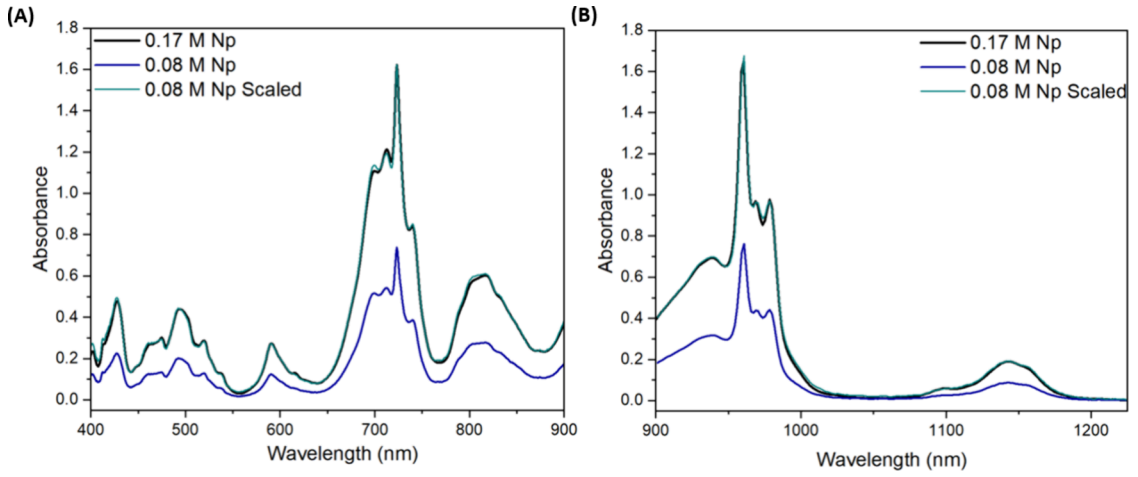

Figure 2. Unscaled and scaled UV−vis (A) and NIR (B) spectra of 0.17 and 0.08 M Np in 1.0 M HNO_3.

tronic f → f transitions are hypersensitive and change in peak shape, intensity, and position as the coordination environment of the actinide changes.

Studies in the literature generally focus on Np(IV) nitrate speciation based on increasing the HNO_3 concentration in three primary groups. Friedman and Toth[8] reported spectra of Np(IV) in 0.1 to 4 N HNO_3. Studies have attributed the spectral features of Np in this acid range to "lower nitrate Np(IV) species," such as mono- and dinitrato species; however, more studies are needed to confirm this assignment.[8,19−21] Spectra of Np(IV) from 6.0 to 15.5 M HNO_3 reported by Ryan[9] show continued changes in the spectral features, with the stabilization of the hexanitrato species beginning at approximately 7 M HNO_3 and the pure hexanitrato species observed at 14 M HNO_3 and above. Although HNO_3 concentrations below 6 M were not reported in this study, Ryan suggested that spectra of Np(IV) in 5 M HNO_3 and below can be attributed to a singular lower Np(IV) nitrate species.

However, other spectrophotometric, complexation, and EXAFS studies suggest that this system is more complex. Rykov et al.[22] proposed three primary regions of speciation based on spectrophotometric data, with the hydrated Np(IV) cation dominating at $[NO_3^-] < 1$ M, an intermediate Np(IV)−nitrate species dominant between 1 M < NO_3^- < 8 M, and the hexanitrato complex dominant at $[NO_3^-] \geq 8$ M. Speciation diagrams also suggest more complicated speciation than the two-species model proposed by Ryan, particularly at low to intermediate $[HNO_3]$.

Based on the literature, the spectra in Figure 1 can be grouped into three acid ranges: 0.5−1.0, 2.5−6.0, and 7.0−10.0 M. For each of these spectra, the primary regions that change the most are between approximately 650−750 nm in UV−vis and between 900−1050 nm in NIR. Changes in the UV−vis region, particularly near 720 nm, are consistent with the study of Friedman and Toth; however, in the study of Chatterjee et al., these changes were not observed.[8,10] Notably, these studies used either chemical (Friedman and Toth) or electrochemical (Chatterjee et al.) methods to stabilize Np(IV).

The spectrum in 0.5 M HNO_3 (black trace) is largely identical to that of Np in $HClO_4$, which is consistent with the presence of the Np(IV) hydrated ion because $HClO_4$ is a noncomplexing medium.[5,22] Increasing the acid concentration to 1.0 M HNO_3 does not significantly change the corresponding spectral features, although the primary peaks at approximately 723 and 960 nm decrease in intensity, while the shoulders at 698, 712, 970, and 978 nm slightly increase in intensity. Although speciation diagrams from Lahr and Knoch and Moskvin suggest the formation of cationic and neutral Np(IV) nitrate species, the exact speciation of Np(IV) at this concentration is uncertain.[19,20] However, EXAFS data from Ikeda-Ohno et al. demonstrated that as nitrate concentration increases, nitrate groups coordinate the Np(IV) ion and displace the coordinated water molecules.[11] The changes in spectral features over this HNO_3 concentration range are likely due to this complexation behavior, although exact peak assignments cannot be made at this time.

For the second range of acid concentrations (2.5−6.0 M HNO_3), the feature at approximately 698 nm is the most intense peak in the UV−vis region. In the NIR, the most intense peak is located at 980 nm. Also, the broad shoulder centered at approximately 938 nm increases in intensity. Intensities of the primary spectral features decrease systematically as acid concentration increases from 4.0 to 6.0 M. Again, formation constants suggest changes in speciation at these concentrations, with tri- and tetranitrato Np(IV) complexes increasing in concentration.[19,20] The origin of these peaks at approximately 720 nm is uncertain and is likely due to multiple Np(IV) nitrate complexes, so we tentatively attribute changes in peak intensities observed here to changes in the concentration of $[Np(NO_3)_n]^{4-n}$ species. In the NIR, the peak at 960 nm has been attributed to the free hydrated Np(IV) ion.[21] This assignment is consistent with our data, in which this signal has gradually decreased in intensity as $[HNO_3]$ increases and nitrate groups coordinate the Np(IV) ion.

In this study, over the acid range of 7.0−10.0 M, corresponding spectral features between 650 and 750 nm also systematically decrease, and a new band at 874 nm increases in intensity with increasing acid concentration. The broad peaks near 808 and 780 nm increase with acid concentration. Ryan observed a peak at 874 nm beginning at 7.0 M HNO_3 that increases in intensity up to 15.5 M HNO_3 and assigned this peak to the Np(IV) hexanitrato complex.[21] The spectrum collected in 10.0 M HNO_3 from this study is consistent with this observation. In the NIR, the peak at approximately 978 nm also broadens with increasing acidity

https://doi.org/10.1021/acsomega.4c05464
ACS Omega 2024, 9, 43547−43556

and the broad signal at 938 nm decreases until it is not observed in the spectrum of the 10.0 M HNO_3 sample. EXAFS data suggest that at 10 M nitrate concentrations, the tetra- and trinitrato Np complexes dominate in solution.[11]

Given that spectral features of tetravalent Np change with varying [HNO_3], a sample with 0.17 M Np in 1.0 M HNO_3 was prepared (S13) to determine if Np(IV) spectra are also sensitive to the Np concentration. This additional sample had approximately two times the Np concentration as S2, and both were prepared in 1.0 M HNO_3 to allow for comparison of the corresponding spectra. Representative spectra for these samples are listed in Figure 2. As shown by the baseline corrected absorbance spectra in Figure 2, the primary difference between the spectra of these two samples is the intensity. The spectrum of the 0.17 M Np sample (black trace) is approximately two times more intense than the spectrum of the 0.08 M Np (blue trace). This intensity difference matches well with the difference in concentration between these two samples. As shown in Figure 2, the spectra are scaled so that an integer of approximately two is multiplied by the intensity values of the spectra corresponding to the 0.08 M Np sample to account for this concentration difference. Upon close examination, the spectral features of these scaled spectra (teal trace) are almost identical. This similarity implies that at these Np and HNO_3 concentrations, spectral features of Np(IV) are not highly dependent upon Np concentration.[15]

The spectra reported here confirm the sensitivity of Np(IV) speciation and absorbance spectra to the HNO_3 concentration. However, peak intensities and shape change rather drastically as a function of HNO_3, and this complexity cannot be accounted for using a univariate model such as Beer's law.[4] Molar extinction coefficients have been reported for Np(IV); however, most focus on low acid concentrations (<2 M).[8,9] To our knowledge, no study has examined changes in molar absorptivity coefficients as a function of the HNO_3 concentration over this range of HNO_3 concentrations for Np(IV) using a consistent method to stabilize this specific oxidation state. Molar absorptivity coefficients were calculated for the most significant spectral features associated with Np(IV) and are listed in Table 2.

PCA of Np(IV) Absorbance Spectra. Despite numerous studies of the Np(IV) nitrate system, uncertainty remains regarding its speciation as a function of the HNO_3 concentration. In this work, we applied PCA to gain insight into Np nitrate speciation over the studied HNO_3 concentration range without using knowledge of the HNO_3 concentrations to build the model since PCA is an unsupervised model.[4] First, PCA was applied to large spectroelectrochemical data sets for each sample to reduce the data and locate representative Np(IV) absorbance spectra for each sample. These spectra are given in Figure 1. PCA scores plots guided the selection of these end point spectra by providing inflection points that reflected the gradual reduction of Np during the electrochemical scan. A representative PCA scores plot is given in Figure S2).[15]

Then, after baseline correcting of the spectra such as those shown in Figure 1, additional PCA models were built. Scores and loadings plots of models built from UV−vis data are given in Figure 3A,B and from the NIR data in Figure 3C,D. The first two principal components (PCs) describe 99.4% of the signal variance for the UV−vis spectra (PC-1:82.58, PC-2:16.86%). The scores and loading plots are used to understand spectral changes in the Np(IV) nitrate system. In Figure 3A, the scores plot shows nine color-coded points, one for each HNO_3 concentration. An inverse trend is observed between HNO_3 concentration and PC-1, with the HNO_3 concentration increasing as the PC-1 value decreases. Interestingly, a cluster of points corresponding to spectra collected from 2.5, 4.0, 5.0, 6.0, and 7.0 M HNO_3 is located near a PC-1 value of approximately 0.5. The corresponding loading plot for PC-1 (Figure 3B, light green trace) displays features close to 720 nm that are similar to features in the spectrum collected in 0.5 M HNO_3. Another identifying feature of the PC-1 loading is the negative peak at 875 nm, which Ryan assigned to the Np hexanitrato complex.[9] The loading plot of PC-1 shows that features from multiple samples are present, indicating that each PC cannot be interpreted as a singular Np(IV) nitrate species. It is also likely that the ratios of complexes that form are constantly changing with acid concentration as no two spectra are exactly the same. This could be the reason for the V-shaped arrangement of points (spectra) in the PCA score plots as opposed to multiple clusters of points that would indicate similar spectra. Both the scores and loadings plots of PC-1 suggest that this PC largely describes HNO_3 concentration.

A V-shaped curve is observed between PC-2 and HNO_3 concentrations. The PC-2 values decrease with increasing HNO_3 concentration until approximately 4.0 M. The cluster of points corresponding to 3.0, 4.0, 5.0, 6.0, and 7.0 M HNO_3 is located at the apex of the V shape and has the highest PC-2 values. As the HNO_3 concentration increases to 8.0 and 10.0 M, the PC-2 values decrease.

The loading plot for PC-2 (Figure 3B) shows that this PC has a significant loading on the band near 724 nm. The corresponding band in the spectral data is rather complex and initially increases in intensity until approximately 5.0 M HNO_3 and then decreases in intensity from 6.0 to 10.0 M HNO_3. Compared with PC-1, the feature in the loading plot of PC-2 at approximately 724 nm decreases in intensity. This decrease again mimics changes observed in the spectra in which the intensity of the peak at approximately 724 nm decreases and broadens with increasing HNO_3 concentration.

For the NIR spectra, the first three PCs explain 99.0% of the signal variance (PC-1:55.26, PC-2:38.80, PC-3:4.92%). The score plot of PC-2 versus PC-1 (Figure 3C) is similar to that of the PCA model built from the UV−vis data. As observed in the PCA score plot of the UV−vis data, the cluster of points corresponding to spectra collected from 4.0 to 7.0 M HNO_3 lies at a PC-1 value close to approximately 0.5. A similar V-

Table 2. Spectral Profiles Were Observed in 0.08 M Np in Varying HNO_3 Concentrations

sample	molar absorptivity (M^{-1} cm^{-1}) at given characteristic electronic transitions						
HNO_3 concentration	700 nm	724 nm	740 nm	938 nm	960 nm	968 nm	976 nm
0.5 M	35	68	29	20	66	29	22
1.0 M	38	54	28	23	54	31	32
2.5 M	40	35	28	24	29	31	41
4.0 M	45	35	31	28	24		49
5.0 M	45	34	30	28	23		47
6.0 M	41	31	27	25			45
7.0 M	38	28	25	23			36
8.0 M	30	21	19	15			24
10.0 M	16		10				13

https://doi.org/10.1021/acsomega.4c05464
ACS Omega 2024, 9, 43547−43556

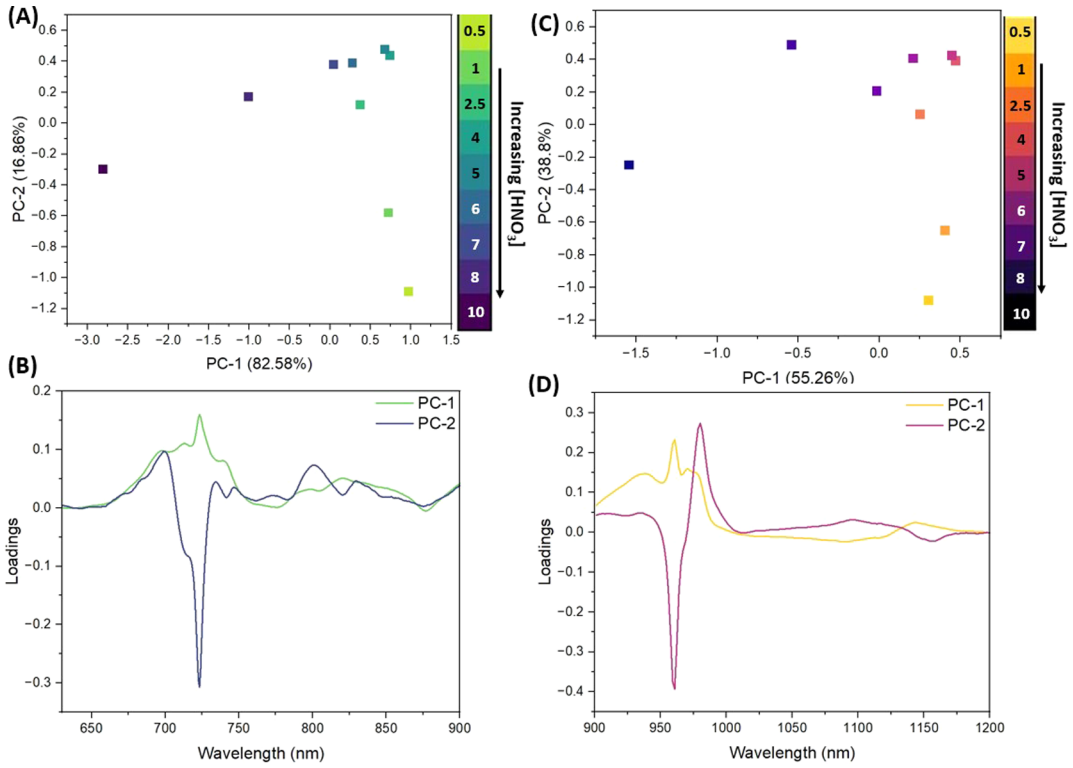

Figure 3. PCA scores and loadings plots from UV−vis (A, B) and NIR (C, D) spectra. The nine HNO_3 concentrations shown in the scores plots correspond to those shown in Table 2 in sequential order.

shape is also observed between PC-1 and PC-2. PC-2 values increase from 0.5 to 4.0 M, with the cluster of points corresponding to spectra collected from 4.0 to 7.0 M HNO_3 located at the apex of the V-shape and decrease in value at 10.0 M HNO_3.

The loadings plots of these two PCs, given in Figure 3D, were used to help interpret the scores plot. For PC-1, a significant loading occurs on the broad signal at 935 nm and the peaks at 960 and 978 nm. Points corresponding to the 0.5 and 10.0 M HNO_3 spectra have the most significant loadings on PC-1. For PC-2, a negative feature is observed at 960 nm and a positive feature is observed at 978 nm. This loading is characteristic of the spectra from 0.5 to 1.0 M, in which the 960 nm peak attributed to the hydrated Np(IV) ion decreases and the peak at 978 nm increases.[5,22]

Both PCA models describe changes in Np(IV) speciation with an increasing HNO_3 concentration. From the score plots, consistent, gradual change is shown in the spectra from 0.5 to 2.5 M HNO_3. Spectra collected in 4.0−7.0 M HNO_3 have very similar PC-1 and PC-2 values, suggesting that these spectra, and likely their speciation, are also similar. The points corresponding to spectra collected from 8.0 to 10.0 M HNO_3 are not positioned closely to the rest of the data set. This suggests significant spectral changes that likely arise from changes in the speciation. Although the exact speciation cannot be gleaned from these plots, this change indicates that our data can be considered in three main groups: 0.5−2.5, 4.0−7.0, and 8.0−10 M HNO_3. This grouping aligns with the study from Rykov et al. that suggested that Np(IV) nitrate speciation falls into three primary acid ranges.[22]

Some details about speciation can be interpreted from the PCA loading plots of the most significant PCs, such as features from multiple spectra appearing in a single loadings plot. As such, each PC cannot be interpreted as a distinct species. Other techniques, such as multivariate curve resolution and PLS discriminant analysis, were applied to the data in this study but had similar results. Multivariate curve resolution output suggests three components; however, the solutions were ambiguous, even when external constraints (e.g., non-negativity) were included. The analysis provides an approximation concentration and spectral components, but the method suffers from rotational ambiguity, suggesting that the spectral response in the Np(IV) system is more complex than Pu(IV).[6]

PLSR and SVR Model Optimization. Linear PLSR and nonlinear SVR models were built and compared to see which can more accurately predict the HNO_3 concentration. PLSR models are built from a signal matrix and a response matrix. In this case, the signal matrix consists of the spectra, and the response matrix consists of the HNO_3 concentrations at which each of those spectra was collected.[12] The use of PLS and SVR to quantify analyte concentrations, such as HNO_3, has been demonstrated previously for both transition metal and actinide nitrate systems.[16,23−25] Because PLSR and SVR include a response matrix, they are considered supervised models.[4]

Similar to the PCA models described previously, two regions from the UV−vis and NIR spectra were modeled separately and compared. Because this data set is rather complex, the initial models included spectra from all 13 samples in the calibration set (Vis 13 model). These models were used to test and optimize the spectral range and preprocessing routine used for model building and to identify a suitable CV technique. Spectral ranges that emphasize significant spectral features that change as a function of HNO_3 give the best models. The leave-one-out CV technique is appropriate for model CV due to the small number of samples in the training set. Based on the

https://doi.org/10.1021/acsomega.4c05464
ACS Omega 2024, 9, 43547−43556

Table 3. RMSE Calibration, CV, and Prediction Metrics for Nitric Acid (0.5−10 M) for the PLSR and SVR Sub-Models Built from Vis Data

model	model type (F/ε,γ)	RMSEC%	RMSECV%	RMSEP%	SEP	bias
Vis 13	PLSR1 (6)	1.5	18.5			
	SVR (3,19)	*2.1*	*14*			
Vis 12	PLSR1 (6)	2.1	8.9	22	N/A	1.0
	SVR (3,8)	*2.0*	*16*	*7.5*	*N/A*	*0.36*
Vis 11	PLSR1 (6)	2.1	11	15	0.56	0.29
	SVR (3,11)	*2.0*	*16*	*5.8*	*0.38*	*0.061*
Vis 10	PLSR1 (6)	1.3	15	13	0.58	0.40
	SVR (1,9)	*2.2*	*16*	*5.1*	*0.29*	*0.0036*
Vis 9	PLSR1 (6)	1.6	19	9.4	0.48	0.17
	SVR (4,7)	*2.1*	*18*	*4.7*	*0.21*	*−0.13*
Vis 8	PLSR1 (6)	1.3	11	18	0.63	0.63
	SVR (4,5)	*2.3*	*18*	*7.6*	*0.39*	*0.11*

RMSE plots, six LVs were included in the UV−vis-based model, and five LVs were included in the NIR-based model. For the UV−vis model, 99.92% of the *Y*-variance can be explained by six LVs. For the NIR-based PLSR models, 99.13% of the *Y*-variance can be explained by five LVs. Given the significant number of potential Np nitrato complexes in this system and potential interactions between them, 5 or 6 LVs were reasonable. Fewer LVs were evaluated for both UV−vis and NIR models; however, these models do not give reasonable percent RMSEP values. The difference between RMSEC and RMSECV values suggests that leaving samples out of this training set significantly affects the performance.

Analogous SVR models were also built and evaluated. SVR is a regression technique that uses loss functions to determine support vectors that describe the variance in a data set.[13,17,18] In this study, C-SVR was used to build and train models for the prediction. First-, second-, and third-order polynomials and a radial basis function were tested. The third-order polynomial allowed for the selection of optimal ε and γ values that produced balanced RMSEC and RMSECV values.

Comparison of Models Built with Varying Numbers of Samples. Once calibration and CV methods were optimized with the 13 sample models, the number of samples included in the calibration set was decreased (Vis, 12, 11, 10, 9, and 8 models). To determine the minimum number of samples to include in the predictive models without compromising the predictive ability, additional models were built with one sample successively removed from the calibration set and put in the validation set. Multiple models were built, and the number of samples in this independent set increased as the number of samples in the calibration set decreased. For example, for the eight-sample model (Vis 8), eight samples were included in the calibration set, and the five samples that were removed comprised the validation set (see Table S1 for information about calibration and validation sets for each model). To be consistent with the initial models that included spectra of all 13 samples, the number of LVs was kept consistent for all PLSR models to allow for a comparison of predictive ability.

PLSR and SVR models built from UV−vis and NIR data were compared to assess which model produces more accurate HNO_3 concentration predictions. Corresponding RMSE values are given for the UV−vis-based PLSR and SVR models in Table 3. Analogous values for NIR-based models are given in Table S2 and Figure S6. The parity plot for the UV−vis-based model built using nine samples is given in Figure 4. Based on RMSE values, the PLSR and SVR models cross-validate

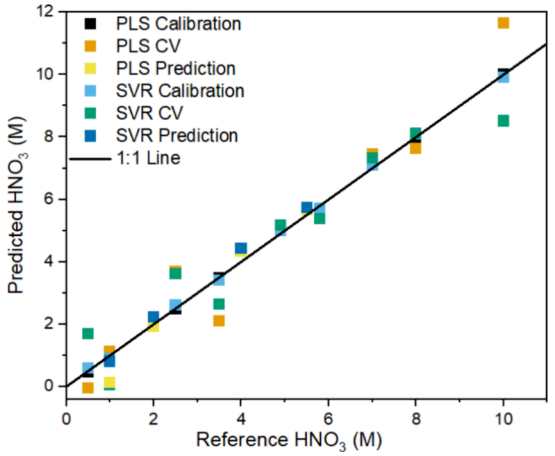

Figure 4. Parity plots of the calibration, CV, and prediction data points for the UV−vis nine-sample (Vis 9) SVR and PLSR models of the Np(IV) UV−vis data.

comparably. However, the SVR model demonstrates better prediction performance than the corresponding PLSR model and gives lower percent RMSEP values. This general trend is observed for all models reported in this study. Previous work defined percent RMSEP values of less than 10% as "satisfactory" and less than 5% as "strong," making this model fall into the latter category.[23] Bias is also important to consider when assessing the strength of a predictive model. When the standard error of prediction (SEP) value is similar to the RMSEP, bias on the model can be regarded as insignificant.[26] For all models, the SEP values for each of the PLSR and SVR models are close to their corresponding RMSEP values, indicating that the bias is insignificant. Based on the CV parity plot in Figure 4, four samples are essential for both model types: 0.5, 2.5, 3.5, and 10 M. The 0.5 and 10 M samples are the bounding points of this data set, and the 2.5 and 3.5 M samples represent low to intermediate acid concentrations, which are located close to the apex seen in the PCA scores plots, indicating their importance for the model to cope with changes in Np(IV) speciation. This result suggests that these four samples are needed to be included in the calibration set. When these samples were left out during the CV process, it led to inflated RMSECV values even though the models demonstrated good predictive ability.

RMSE metrics as a function of the number of samples included in the training set of the model are given in Figure 5,

https://doi.org/10.1021/acsomega.4c05464
ACS Omega 2024, 9, 43547−43556

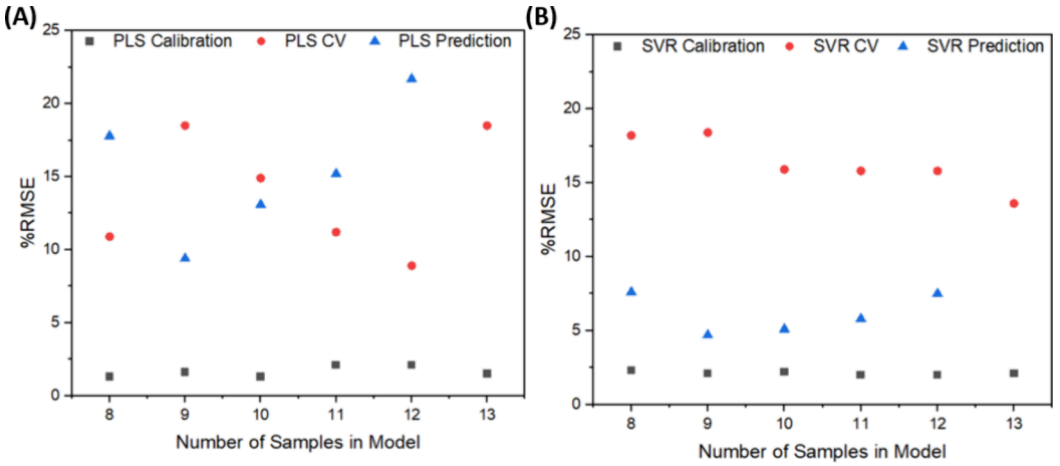

Figure 5. RMSE% values for nitric acid (0.5−10 M) as a function of the number of samples included in the calibration set for (A) PLSR models and (B) SVR models.

and NIR model results are shown in Figure S7. The RMSEC values for the PLSR and SVR models built from UV−vis data are comparable, and PLSR models generally have more sporadic RMSECV values than those of the SVR models. As mentioned previously, inflated RMSECV values are attributed to the removal of the two bounding points, 0.5 and 10.0 M, and two low to intermediate acid concentrations, 2.5 and 3.5 M, during CV. However, the largest difference between the PLSR and SVR models of the UV−vis data is their predictive ability. In comparing the percent RMSEP values of these two model types, the PLSR models generally fall at or above the "satisfactory" rating (>10%). For the SVR models, the percent RMSEP values for all models fall within the "strong" to "satisfactory" ratings. This result implies that the SVR models have better predictive ability than the corresponding PLSR models even though the PLSR models generally cross-validated better than the SVR models. This result also suggests that spectra of all HNO_3 concentrations in the data set are significant and that leaving one HNO_3 concentration out significantly affects the performance of the model. Additional discussion of the NIR-based PLSR and SVR models is given in the SI.

Importantly, the number and identity of the samples that were removed from the training set and put in the validation set greatly affected the predictive ability of the model. Models built and calibrated using nine to ten samples appear to produce reasonable RMSE values that are calibrated, validated, and predicted well. Metrics of models that contained eight samples in the calibration set and five samples in the validation set also show good prediction capability, although not as strong as the nine- and ten-sample models. The identities of the samples removed from the calibration set also affect the predictive ability. Analogous models that removed the spectra collected in 3.5 M HNO_3 from the calibration set (not shown here) perform poorly and have higher percent RMSEP values compared with models that retained this data point in the calibration set. A similar effect is also observed with the removal of the spectra collected in 2.0 M HNO_3 from the training set. This observation suggests that spectra collected in the low to intermediate acid concentration range are particularly important, perhaps describing significant changes in the speciation of Np(IV) that are needed for the model to perform well.

This work evaluated whether it is possible to build a single predictive model to cover a large range of HNO_3 concentrations. The nonlinear spectral response is best modeled using SVR. In practice, it may be advantageous to build local regression models with sample sets covering narrower acid ranges or employ hierarchical or locally weighted techniques to cover a wide range of HNO_3 levels, which could be explored in future work.

CONCLUSIONS

The results of this study underscore the complexity of Np(IV) absorbance spectra as a function of the HNO_3 concentration. Spectra were collected from acidic solutions in which Np(IV) was stabilized electrochemically. Corresponding molar absorptivity coefficients were calculated for the most significant Np(IV) absorbance bands. Spectra were used to build PCA, PLSR, and SVR models. Data reduction using PCA was successful in guiding the selection of Np(IV) endpoint spectra for each acid sample and identifying spectral features of multiple Np(IV) nitrate species that contribute to the variance in the spectral data. Additionally, PCA scores plots suggest that Np(IV) nitrate speciation is complex and that multiple Np nitrate complexes and ratios of these complexes form over the acid concentration range studied here. While spectra collected from 4 to 7 M HNO_3 have similar spectral features, clear clusters of points are not observed in these scores plots. Acid concentration was confirmed as the most significant contributor to variance in the data set.

To assess the best method for the predictive capability of such a complex data set, PLSR and SVR were directly compared. Nonlinear SVR models had better predictive abilities than linear PLSR models for both the UV−vis and NIR data sets, as evidenced by percent RMSEP values less than 5%. Additionally, SVR models built with UV−vis spectral data generally had lower percent RMSEP values and better predictive ability than the corresponding SVR models built with NIR spectra. This study also observed that percent RMSEC and percent RMSECV values are not necessarily good indicators of predictive capability. The outcomes of this study are highly relevant to nuclear processing, especially for the potential of Np(IV) to be used as a probe for HNO_3 concentration, which is a critical parameter that requires careful control during radioisotope purification.[15,27] In a

https://doi.org/10.1021/acsomega.4c05464
ACS Omega 2024, 9, 43547−43556

broader sense, these findings also have the capability to affect other metal nitrate systems, such as transition metal systems. Future work will focus on modeling spectra with dynamic temperature and varying total Np concentration because both are significant factors that heavily influence processing conditions.[7] The ability to correlate and predict conditions such as actinide concentration, acid concentration, and temperature with spectral data has the potential to affect processing outcomes and make these procedures more efficient.

■ ASSOCIATED CONTENT

Supporting Information

The Supporting Information is available free of charge at https://pubs.acs.org/doi/10.1021/acsomega.4c05464.

Additional absorbance spectra and tables, graphs, and discussion of multivariate models (PDF)

■ AUTHOR INFORMATION

Corresponding Author

Luke R. Sadergaski − *Radioisotope Science and Technology Division, Oak Ridge National Laboratory, Oak Ridge, Tennessee 37831, United States;* orcid.org/0000-0003-0248-2114; Phone: +1 (865) 574-1167; Email: sadergaskilr@ornl.gov

Authors

Sara E. Gilson − *Radioisotope Science and Technology Division, Oak Ridge National Laboratory, Oak Ridge, Tennessee 37831, United States*

Hunter B. Andrews − *Radioisotope Science and Technology Division, Oak Ridge National Laboratory, Oak Ridge, Tennessee 37831, United States;* orcid.org/0000-0002-2091-9415

Adam J. Parkison − *Radioisotope Science and Technology Division, Oak Ridge National Laboratory, Oak Ridge, Tennessee 37831, United States*

Complete contact information is available at: https://pubs.acs.org/10.1021/acsomega.4c05464

Author Contributions

The manuscript was written through contributions of all authors. All authors have given approval to the final version of the manuscript.

Funding

Funding for this research was provided by the Science Mission Directorate of NASA and administered by the U.S. Department of Energy, Office of Nuclear Energy, under contract DEAC05- 00OR22725. S.E.G. would like to acknowledge the Glenn T. Seaborg Initiative for support. This work used the facilities and resources at the Radiochemical Engineering Development Center operated by the US Department of Energy's Oak Ridge National Laboratory.

Notes

The authors declare no competing financial interest.

■ ACKNOWLEDGMENTS

The authors wish to the Cannon Giglio for helpful discussions regarding chemometrics. S.E.G. wishes to thank Samantha Schrell for helpful discussions regarding actinide spectrophotometry. This work was supported by the ^{238}Pu Supply Program at Oak Ridge National Laboratory.

■ ABBREVIATIONS

CV, cross validation; EXAFS, extended X-ray absorption fine structure; LV, latent variable; NIR, near-infrared; PC, principal component; PCA, principal component analysis; PLS, partial least-squares; PLSR, partial least-squares regression; RMSE, root-mean-square error; RMSEC, root-mean-square error of calibration; RMSECV, root-mean-square error of cross validation; RMSEP, root-mean-square error of prediction; SEP, standard error of prediction; SVR, support vector regression; UV, ultraviolet; UV−vis, ultraviolet−visible

■ REFERENCES

(1) Bryan, S. A.; Levitskaia, T. G.; Johnsen, A. M.; Orton, C. R.; Peterson, J. M. Spectroscopic monitoring of spent nuclear fuel reprocessing streams: an evaluation of spent fuel solutions via Raman, visible, and near-infrared spectroscopy. *Radiochim. Acta* **2011**, *99* (9), 563−572. (acccessed 2023−06−01).

(2) Sadergaski, L. R.; Myhre, K. G.; Delmau, L. H. Multivariate chemometric methods and Vis-NIR spectrophotometry for monitoring plutonium-238 anion exchange column effluent in a radiochemical hot cell. *Talanta Open* **2022**, *5*, No. 100120.

(3) Sadergaski, L. R.; DePaoli, D. W.; Myhre, K. G. Monitoring the Caustic Dissolution of Aluminum Alloy in a Radiochemical Hot Cell Using Raman Spectroscopy. *Appl. Spectrosc.* **2020**, *74* (10), 1252−1262. Artn 0003702820933616

(4) Kirsanov, D.; Rudnitskaya, A.; Legin, A.; Babain, V. UV−Vis spectroscopy with chemometric data treatment: an option for on-line control in nuclear industry. *J. Radioanal. Nucl. Chem.* **2017**, *312* (3), 461−470.

(5) Yoshida, Z.; Johnson, S. G.; Kimura, T.; Krsul, J. R. Neptunium. In *The Chemistry of the Actinide and Transactinide Elements*; Morss, L. R.; Edelstein, N. M.; Fuger, J., Eds.; Springer: Netherlands, 2011; pp 699−812.

(6) Lines, A. M.; Adami, S. R.; Sinkov, S. I.; Lumetta, G. J.; Bryan, S. A. Multivariate Analysis for Quantification of Plutonium(IV) in Nitric Acid Based on Absorption Spectra. *Anal. Chem.* **2017**, *89* (17), 9354−9359.

(7) Andrews, H. B.; Sadergaski, L. R. Hierarchical Modeling to Enhance Spectrophotometry Measurements—Overcoming Dynamic Range Limitations for Remote Monitoring of Neptunium. *Chemosensors* **2023**, *11* (5), 274.

(8) Friedman, H. A.; Toth, L. M. Absorption spectra of Np(III), (IV), (V) and (VI) in nitric acid solution. *J. Inorg. Nucl. Chem.* **1980**, *42* (9), 1347−1349.

(9) Ryan, J. L. SpeciesInvolved in the Anion-Exchange Absorption of Quadrivalent Actinide Nitrates. *J. Phys. Chem.* **1960**, *64* (10), 1375−1385.

(10) Chatterjee, S.; Bryan, S. A.; Casella, A. J.; Peterson, J. M.; Levitskaia, T. G. Mechanisms of neptunium redox reactions in nitric acid solutions. *Inorg. Chem. Front.* **2017**, *4* (4), 581−594.

(11) Ikeda-Ohno, A.; Hennig, C.; Rossberg, A.; Funke, H.; Scheinost, A. C.; Bernhard, G.; Yaita, T. Electrochemical and Complexation Behavior of Neptunium in Aqueous Perchlorate and Nitrate Solutions. *Inorg. Chem.* **2008**, *47* (18), 8294−8305.

(12) Wold, S.; Sjöström, M.; Eriksson, L. PLS-regression: a basic tool of chemometrics. *Chemometr. Intell. Lab. Syst.* **2001**, *58* (2), 109−130.

(13) Deiss, L.; Margenot, A. J.; Culman, S. W.; Demyan, M. S. Tuning support vector machines regression models improves prediction accuracy of soil properties in MIR spectroscopy. *Geoderma* **2020**, *365*, No. 114227.

(14) Zuo, Y.; Deng, Y. The near-UV absorption constants for nitrite ion in aqueous solution. *Chemosphere* **1998**, *36* (1), 181−188.

(15) Sadergaski, L. R.; Andrews, H. B.; Gilson, S. E.; Parkison, A. J. Quantifying neptunium oxidation states in nitric acid through spectroelectrochemistry and chemometrics. *Front. Nucl. Eng.* **2023**, *2*, No. 1323372.

(16) Lascola, R.; O'Rourke, P. E.; Kyser, E. A. A Piecewise Local Partial Least Squares (PLS) Method for the Quantitative Analysis of Plutonium Nitrate Solutions. *Appl. Spectrosc.* **2017**, *71* (12), 2579−2594.
(17) Rodríguez-Pérez, R.; Bajorath, J. Evolution of Support Vector Machine and Regression Modeling in Chemoinformatics and Drug Discovery. *J. Comput.-Aided Mol. Des.* **2022**, *36* (5), 355−362.
(18) Rodríguez-Pérez, R.; Vogt, M.; Bajorath, J. Influence of Varying Training Set Composition and Size on Support Vector Machine-Based Prediction of Active Compounds. *J. Chem. Inf. Model.* **2017**, *57* (4), 710−716.
(19) Lahr, H.; Knoch, W. Bestimmung von Stabilitätskonstanten einiger Aktinidenkomplexe. *J. Radiochim. Acta* **1970**, *13* (1), 1−5. (acccessed 2024−03−22).
(20) Moskvin, A. I. Complexing of neptunium(IV) and plutonium-(IV) in nitrate solutions. *Zh. Neorg. Khim.* **1971**, *16*, 759−764.
(21) Barbanel, Y. A. Complexing of neptunium(IV) with nitrate ion studied by a spectrophotometric method. *Radiokhimiya* **1972**, *14*, 489−492.
(22) Rykov, A. G.; Blokhin, N. B.; Vasil'ev, V. Y. Spectrophotometric investigation into complexing and solvation of actinides ions. *Radiokhimiya* **1973**, *15* (3), 341−347.
(23) Andrews, H. B.; Sadergaski, L. R. Leveraging visible and near-infrared spectroelectrochemistry to calibrate a robust model for Vanadium(IV/V) in varying nitric acid and temperature levels. *Talanta* **2023**, *259*, No. 124554.
(24) Felmy, H. M.; Bessen, N. P.; Lackey, H. E.; Bryan, S. A.; Lines, A. M. Quantification of Uranium in Complex Acid Media: Understanding Speciation and Mitigating for Band Shifts. *ACS Omega* **2023**, *8* (44), 41696−41707.
(25) Sadergaski, L. R.; Hager, T. J.; Andrews, H. B. Design of Experiments, Chemometrics, and Raman Spectroscopy for the Quantification of Hydroxylammonium, Nitrate, and Nitric Acid. *ACS Omega* **2022**, *7* (8), 7287−7296.
(26) Faber, N. K. M. A closer look at the bias-variance trade-off in multivariate calibration. *J. Chemomet.* **1999**, *13*, 185−192.
(27) Casella, A. J.; Ahlers, L. R. H.; Campbell, E. L.; Levitskaia, T. G.; Peterson, J. M.; Smith, F. N.; Bryan, S. A. Development of Online Spectroscopic pH Monitoring for Nuclear Fuel Reprocessing Plants: Weak Acid Schemes. *Anal. Chem.* **2015**, *87* (10), 5139−5147.

https://doi.org/10.1021/acsomega.4c05464
ACS Omega 2024, 9, 43547−43556